

Optimized tDCS for Targeting Multiple Brain Regions: An Integrated Implementation*

Yu Huang^{1,2}, Chris Thomas¹, Abhishek Datta¹, and Lucas C. Parra²

Abstract—Transcranial direct current stimulation (tDCS) aims to deliver weak electric current into the brain to modulate neural activities. Based on the volume conductor model of the head, optimization algorithm can be used to determine a specific montage of high-definition electrodes on the scalp to achieve targeted stimulation. However, simultaneous targeting for multiple disconnected regions can rarely be found in the literature. Here we attempted to provide an integrated solution for optimized tDCS to target multiple brain regions (either a single point or brain structures). By improving the “max-intensity” routine previously published in [1], we are able to target two regions of interest (ROI) in the brain simultaneously. For ROIs more than two, we show that the “max-focality” algorithm using weighted least-square in [1] can be further improved by putting the L1-norm constraint on the stimulation current as a penalty term into the cost function. Up to five ROIs can be targeted at the same time without violating the safety criteria. Further analysis shows that, for multiple targets, a trade-off exists between targeting accuracy and the number of electrodes needed. We implemented all these algorithms in Soterix software HD-TargetsTM.

I. INTRODUCTION

Transcranial direct current stimulation (tDCS) delivers weak electric current (0.2 mA to 2 mA) into the brain to modulate neural activities [2]. Research has shown that tDCS can improve performance in some learning tasks and has also shown promise as a potential therapy for a number of neurological disorders such as depression, fibromyalgia and stroke [3], [4], [5], [6]. Compared to conventional tDCS that uses saline-soaked large pad sponges (25–35 cm²) [2], high-definition tDCS (HD-tDCS) leverages a number of small (~75 mm²) gel-based ring electrodes [7], [8]. Modeling studies have shown that HD-tDCS can improve the focality of the stimulation [9], [10]. HD-tDCS provides flexibility in placing multiple electrodes on the scalp. Based on the current-flow models of the head [8], [11], targeted stimulation can then be achieved by using an optimal montage of HD electrodes, which is determined by general-purpose algorithms for optimization problems [1], [12], [13]. They can guide the electric current to a specific brain region (a single point or a brain structure).

However, to the best of our knowledges, simultaneous targeting for multiple disconnected brain regions can be hardly found in the literature. Ref. [1] was the first work

on the optimized tDCS presented with strict mathematical formulation that incorporates the safety constraints, but the proposed algorithms were only applied to guide the current to a single, point-like target. Ref. [12] extends the algorithm of weighted least square in [1] to multiple disconnected cortical targets. Ref. [13] also generalizes the “max-intensity” algorithm in [1] from a point-like target to a brain structure, but it does not explicitly demonstrate this capability of structural targeting to multiple regions.

Here we aim to provide an integrated solution of simultaneously targeting multiple brain regions including both point-like targets and cortical structures. Specifically, we show that the “max-intensity” algorithm in [1] can be improved to target two regions of interest (ROI), by maximizing the L1-norm of the electric field at the targets. For targeting more than two ROIs, the “max-focality” algorithm in [1] based on weighted least square with L1-norm constraint on the stimulation current can be applied and improved by putting the constraint as a penalty term in the cost function. We also demonstrate that there is an intrinsic trade-off between the targeting accuracy and the number of electrodes needed for multiple ROIs. The implementation was integrated into the proprietary software HD-TargetsTM by Soterix Medical (New York, NY).

II. METHODS AND RESULTS

A. Construction of the head model

The ICBM152 (v6) template from the Montreal Neurological Institute (MNI, Montreal, Canada [14], [15]) was used for all the simulations in this work. The computational head models were built following our previous work [11]. Briefly, the ICBM152 (v6) template MRI (magnetic resonance image) was segmented by the New Segment toolbox [16] in Statistical Parametric Mapping 8 (SPM8, Wellcome Trust Centre for Neuroimaging, London, UK) implemented in Matlab (R2013a, MathWorks, Natick, MA). Segmentation errors such as discontinuities in CSF and noisy voxels were corrected first by a customized Matlab script [11] and then by hand in an interactive segmentation software ScanIP (v4.2, Simpleware Ltd, Exeter, UK). Since tDCS modeling work has demonstrated the need to include the entire head down to the neck for realistic current flow, in particular in deep-brain areas and the brainstem [11], the field of view (FOV) of the ICBM152 (v6) MRI was extended down to the neck by registering and reslicing the standard head published in [11] to the voxel space of ICBM152 (see [17] for details). HD electrodes following the convention of the standard 10–10 international system [18] were placed on the scalp surface

*This work was supported by the NIH Grant 5R44NS092144-03.

¹Y. Huang, C. Thomas and A. Datta are with Research & Development, Soterix Medical, Inc., New York, NY 10001, USA yhuang at soterixmedical.com

²Y. Huang and L.C. Parra are with the Department of Biomedical Engineering, City College of the City University of New York, New York, NY 10031, USA yhuang16 at citymail.cuny.edu

by custom Matlab script [11]. Two rows of electrodes below the ears and four additional electrodes around the neck were also placed to allow for targeting of deeper cortical areas and for the use of distant reference electrodes in tDCS. A total of 93 electrodes were placed. A finite element model (FEM, [19]) was generated from the segmentation data by the ScanFE module in ScanIP. Laplace’s equation was then solved [20] in Abaqus 6.11 (SIMULIA, Providence, RI) for the electric field distribution in the head. With one fixed reference electrode Iz as cathode, the electric field was solved for all other 92 electrodes with unit current density injected for each of them, giving 92 solutions for electric field distribution representing the “forward model” or “lead field” of the ICBM152 head. This model will be used for the multi-focal targeting algorithms described below.

B. Multi-focal targeting algorithms

Based on the framework presented in [1], we show here how multiple brain regions can be simultaneously stimulated. Figure 1 and Figure 2 show all the results of targeting multiple locations in the head. The algorithms used are described as equations above each plot. In the equations, \vec{s} is the solution vector indicating the dose of injected current at each electrode (indexed by m), with s_{\max} being the maximal allowed current intensity in tDCS (usually 2 mA). \vec{A} is the lead field computed from the head model (Section II-A). \vec{C}_i is the lead field at target location i . \vec{e}_d is the desired electric field distribution specified by the users. \vec{u}_i is the desired field orientation at target i . N is the number of targets. For details on the notations, one is referred to [1].

The “max-intensity” routine in [1] cannot even target two regions of interests (ROI) simultaneously (Eq. (1), Figure 1(a)). By maximizing the sum of *absolute* values of the electric fields (i.e., the L1 norm) at the ROIs (Eq. (2) in Figure 1, L1-norm maximization was implemented following Algorithm 1 in [21]), the algorithm can achieve maximal intensities for two ROIs (Figure 1(b)), but still cannot perform well for more than two ROIs (Figure 1(e)(h)). In fact, for ROIs more than two, the weighted least-square algorithm in [1] (Eq. (3) in Figure 1) gives better results: the induced electric field is more focal and intense (the total achieved electric field magnitude (regardless of its orientation) summed across all target nodes increases from 2.43 V/m to 2.60 V/m for 3 targets (Figure 1(e)(f)), and from 2.60 V/m to 3.39 V/m for 4 targets (Figure 1(h)(i))).

However, the least-square results in Figure 1 are not feasible in practice, as it violates the safety criteria in tDCS where the total injected current should not exceed 2 mA. This safety requirement can be easily implemented by adding an L1-norm constraint on the delivered current, which is already done in [1] for a single point-like target. Here we implemented the same least-square algorithm with L1-norm constraint (Eq. (4) in Figure 2), but for multiple targets. It shows that fairly focal stimulation can also be achieved simultaneously at multiple brain regions, while at the same time the safety criteria is ensured (Figure 2(a)(c)). Note by enforcing the safety requirement, the total achieved electric

field intensity at all targets is reduced (comparing Figure 1(i) and Figure 2(a); dropped from 3.39 V/m to 0.86 V/m). Furthermore, if we put the L1-norm constraint $\sum_{m=1}^M |s_m| \leq s_{\max}$ into the cost function as in Eq. (5) in Figure 2, a better solution can be obtained: the total achieved electric field magnitude at all target nodes increases from 0.86 V/m to 1.01 V/m for 4 targets (Figure 2(a)(b)), and from 1.00 V/m to 1.13 V/m for 5 targets (Figure 2(c)(d)). The price paid for this improvement is the increase in the number of electrodes needed (Figure 2; from 14 to 28 electrodes for 4 targets, and to 30 electrodes for 5 targets). Further analysis shows that there is an intrinsic trade-off between the accuracy of the electric field distribution under multi-focal targeting and the number of electrodes used (Figure 3, shown for the case of five targets). This is dictated by the parameter λ in the penalty term in Eq. (5). The best λ is chosen at the point close to where the two curves intersect ($\lambda = 0.01$).

With λ set to its optimal value (0.01) for five targets, we show that the weighted least square with L1-norm penalty (Eq. (5) in Figure 2) can be used for targeting not only point-like ROIs, but also brain structures (Figure 4). The parcellation data from the Human Connectome Project (HCP) was used. Specifically, 360 brain structures as presented in [22] were mapped to the voxel space of ICBM152 (v6) MRI. When targeting a specific structure, all the voxels in that region were assigned the desired electric field intensities with the same weights, and then provided to the algorithm to solve for the optimal montage. Compared to targeting point-like locations (Figure 4(a)), slightly more electrodes are needed to target structures, with achieved total electric field intensity being smaller (Figure 4(b)). Note for structural targeting, the mean field intensity achieved at each target was used for computing the total achieved field intensity across targets.

III. CONCLUSIONS AND DISCUSSION

We attempt to provide an integrated solution for optimized tDCS to target multiple brain regions simultaneously. It works for both point-like and structural targets, and computes fast (in fewer than one minute). We implement the algorithms in Soterix software HD-Targets™.

It turned out that the weighted least-square penalized by L1-norm of the delivered current (Eq. (5)) is the best method for multi-focal targeting. The intensity at each target becomes lower when the number of targets increases (Figure 2(b)(d), from four targets to five, average intensity at each target drops from 0.25 V/m to 0.23 V/m). This is dictated by the physics of the head anatomy and the HD electrodes setup. A trade-off between accuracy and practicality exists for multi-focal targeting (Figure 3). Since in practice tDCS device with more than 8 channels is hard to implement, there are efforts trying to reduce the number of electrodes in the optimal montage output by the targeting algorithms, giving sub-optimal solutions. For example, Ref. [12] used genetic algorithm to calculate the optimal number of electrodes; Ref. [23] explored the branch and bound algorithm to find sub-optimal electrode montage with only up to 3 current sources. However, these are very computationally expensive (takes

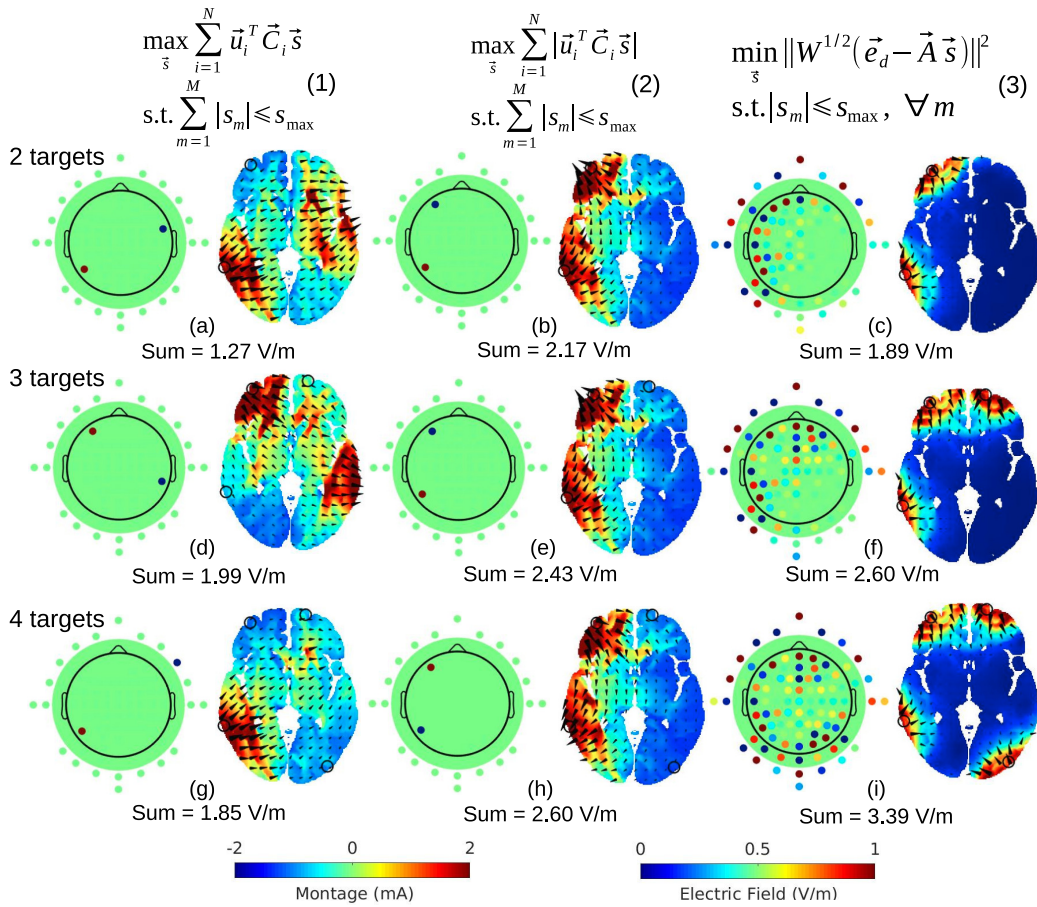


Fig. 1. Optimized tDCS simulations on the ICBM152 (v6) head for different number of targets and different algorithms. Targets are indicated by black circles on the slice plot. The dose in the electrode montage and electric field distribution refer to the two colormaps at the bottom, respectively. The sum of electric field intensities across targets are noted below each plot.

hours to compute). Currently with Soterix $M \times N - 32$ HD-tES device that supports up to 32 channels, it seems that targeting up to five brain regions at the same time is feasible in practice (30 electrodes needed, Figure 2(d)). Moreover, one can always sacrifice the accuracy a little bit for fewer electrodes (Figure 3), and the tuning of this accuracy–practicality is not computationally intensive (only takes several minutes).

ACKNOWLEDGMENT

The authors would like to thank Jacek Dmochowski for fruitful discussions on the targeting algorithms. This work was supported by the NIH Grant 5R44NS092144-03.

REFERENCES

- [1] J. P. Dmochowski, A. Datta, M. Bikson, Y. Su, and L. C. Parra, “Optimized multi-electrode stimulation increases focality and intensity at target,” *Journal of Neural Engineering*, vol. 8, no. 4, p. 046011, Aug. 2011.
- [2] M. A. Nitsche and W. Paulus, “Excitability changes induced in the human motor cortex by weak transcranial direct current stimulation,” *The Journal of Physiology*, vol. 527, no. 3, pp. 633–639, Sep. 2000.
- [3] M. A. Nitsche, A. Schauenburg, N. Lang, D. Liebetanz, C. Exner, W. Paulus, and F. Tergau, “Facilitation of implicit motor learning by weak transcranial direct current stimulation of the primary motor cortex in the human,” *Journal of Cognitive Neuroscience*, vol. 15, no. 4, pp. 619–626, 2003.
- [4] F. Fregni, R. Gimenes, A. C. Valle, M. J. L. Ferreira, R. R. Rocha, L. Natalle, R. Bravo, S. P. Rigonatti, S. D. Freedman, M. A. Nitsche, A. PascualLeone, and P. S. Boggio, “A randomized, sham-controlled, proof of principle study of transcranial direct current stimulation for the treatment of pain in fibromyalgia,” *Arthritis & Rheumatism*, vol. 54, no. 12, pp. 3988–3998, Dec. 2006.
- [5] M. Bikson, P. Bulow, J. Stiller, A. Datta, F. Battaglia, S. Karnup, and T. Postolache, “Transcranial direct current stimulation for major depression: A general system for quantifying transcranial electrotherapy dosage,” *Current Treatment Options in Neurology*, vol. 10, no. 5, pp. 377–385, 2008.
- [6] G. Schlaug, V. Renga, and D. Nair, “Transcranial direct current stimulation in stroke recovery,” *Arch Neurol*, vol. 65, no. 12, pp. 1571–1576, Dec. 2008.
- [7] H.-I. Kuo, M. Bikson, A. Datta, P. Minhas, W. Paulus, M.-F. Kuo, and M. A. Nitsche, “Comparing cortical plasticity induced by conventional and high-definition 4 1 ring tDCS: a neurophysiological study,” *Brain stimulation*, Oct. 2012.
- [8] D. Edwards, M. Cortes, A. Datta, P. Minhas, E. M. Wassermann, and M. Bikson, “Physiological and modeling evidence for focal transcranial electrical brain stimulation in humans: A basis for high-definition tDCS,” *NeuroImage*, vol. 74, pp. 266–275, Jul. 2013.
- [9] A. Datta, V. Bansal, J. Diaz, J. Patel, D. Reato, and M. Bikson, “Gyri-precise head model of transcranial DC stimulation: Improved spatial focality using a ring electrode versus conventional rectangular pad,” *Brain stimulation*, vol. 2, no. 4, pp. 201–207, Oct. 2009.
- [10] J. P. Dmochowski, M. Bikson, and L. C. Parra, “The point spread function of the human head and its implications for transcranial current stimulation,” *Physics in medicine and biology*, vol. 57, no. 20, pp. 6459–6477, Oct. 2012.
- [11] Y. Huang, J. P. Dmochowski, Y. Su, A. Datta, C. Rorden, and L. C.

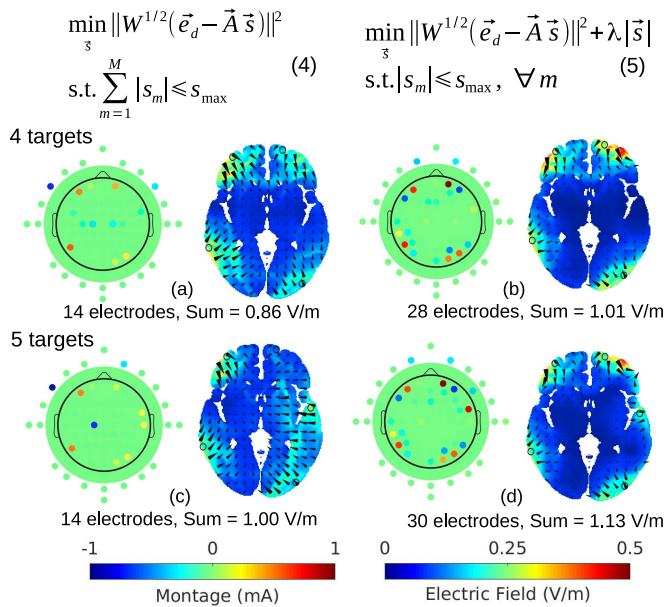


Fig. 2. Targeting on more than three ROIs by weighted least square algorithms with different approaches to safety constraints. Targets are indicated by black circles on the slice plot. The dose in the electrode montage and electric field distribution refer to the two colormaps at the bottom, respectively. The sum of electric field intensities across targets are noted below each plot.

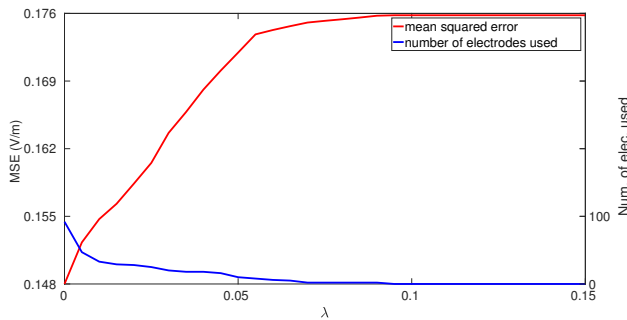


Fig. 3. The trade-off between the accuracy of multi-focal targeting and the number of used electrodes on the scalp. The accuracy is quantified as the mean squared error (MSE) between the desired electric field distribution and the actual achieved one from the algorithm. The results shown are obtained when targeting five ROIs.

Parra, “Automated MRI segmentation for individualized modeling of current flow in the human head,” *Journal of Neural Engineering*, vol. 10, no. 6, p. 0666004, Dec. 2013.

- [12] G. Ruffini, M. D. Fox, O. Ripolles, P. C. Miranda, and A. Pascual-Leone, “Optimization of multifocal transcranial current stimulation for weighted cortical pattern targeting from realistic modeling of electric fields,” *NeuroImage*, vol. 89, pp. 216–225, Apr. 2014.
- [13] S. Guler, M. Dannhauer, B. Erem, R. Macleod, D. Tucker, S. Turovets, P. Luu, D. Erdogmus, and D. H. Brooks, “Optimization of focality and direction in dense electrode array transcranial direct current stimulation (tDCS),” *Journal of Neural Engineering*, vol. 13, no. 3, p. 036020, Jun. 2016.
- [14] J. Mazziotta, A. Toga, A. Evans, P. Fox, J. Lancaster, K. Zilles, R. Woods, T. Paus, G. Simpson, B. Pike, C. Holmes, L. Collins, P. Thompson, D. MacDonald, M. Iacoboni, T. Schormann, K. Amunts, N. Palomero-Gallagher, S. Geyer, L. Parsons, K. Narr, N. Kabani, G. Le Goualher, J. Feidler, K. Smith, D. Boomsma, H. H. Pol, T. Cannon, R. Kawashima, and B. Mazoyer, “A four-dimensional probabilistic atlas of the human brain,” *Journal of the American*

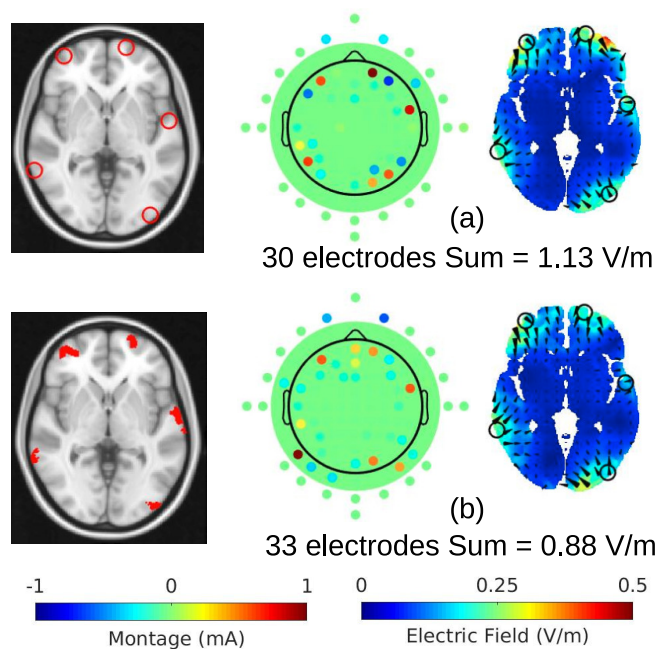


Fig. 4. Targeting on five point-like ROIs (first row, red circles in the MRI) and five brain structures (second row, red regions in the MRI). The dose in the electrode montage and electric field distribution refer to the two colormaps at the bottom, respectively. The sum of electric field intensities across targets are noted below each plot.

Medical Informatics Association : JAMIA, vol. 8, no. 5, pp. 401–430, 2001.

- [15] G. Grabner, A. L. Janke, M. M. Budge, D. Smith, J. Pruessner, and D. L. Collins, “Symmetric atlas and model based segmentation: an application to the hippocampus in older adults,” *Medical image computing and computer-assisted intervention: MICCAI: International Conference on Medical Image Computing and Computer-Assisted Intervention*, vol. 9, no. Pt 2, pp. 58–66, 2006.
- [16] J. Ashburner and K. J. Friston, “Unified segmentation,” *NeuroImage*, vol. 26, no. 3, pp. 839–851, Jul. 2005.
- [17] Y. Huang, L. C. Parra, and S. Haufe, “The new york head – a precise standardized volume conductor model for eeg source localization and tes targeting,” *NeuroImage*, vol. 140, pp. 150 – 162, 2016.
- [18] G. H. Klem, H. O. Lders, H. H. Jasper, and C. Elger, “The ten-twenty electrode system of the international federation. the international federation of clinical neurophysiology,” *Electroencephalography and clinical neurophysiology. Supplement*, vol. 52, pp. 3–6, 1999.
- [19] D. L. Logan, *A First Course in the Finite Element Method*, 4th ed. Toronto: Nelson, 2007.
- [20] D. J. Griffiths, *Introduction to electrodynamics*, 3rd ed. Upper Saddle River, NJ: Prentice Hall, 1999.
- [21] F. Nie, H. Huang, C. Ding, D. Luo, and H. Wang, “Robust principal component analysis with non-greedy l_1 -norm maximization,” in *Proceedings of the Twenty-Second International Joint Conference on Artificial Intelligence - Volume Volume Two*, ser. IJCAI’11. AAAI Press, 2011, pp. 1433–1438.
- [22] M. F. Glasser, T. S. Coalson, E. C. Robinson, C. D. Hacker, J. Harwell, E. Yacoub, K. Ugurbil, J. Andersson, C. F. Beckmann, M. Jenkinson, S. M. Smith, and D. C. Van Essen, “A multi-modal parcellation of human cerebral cortex,” *Nature*, vol. 536, no. 7615, pp. 171–178, 2016.
- [23] S. Guler, M. Dannhauer, B. Erem, R. Macleod, D. Tucker, S. Turovets, P. Luu, W. Meleis, and D. H. Brooks, “Optimizing Stimulus Patterns for Dense Array tDCS With Fewer Sources Than Electrodes Using A branch and Bound Algorithm,” *Proceedings. IEEE International Symposium on Biomedical Imaging*, vol. 2016, pp. 229–232, Apr. 2016.